Applied Nanoscience (2021) 11:9–20
https://doi.org/10.1007/s13204-020-01559-9

ORIGINAL ARTICLE

A comparative study for convective flow of basefluid (gasoline oil), nanomaterial (SWCNTs) and hybrid nanomaterial (SWCNTs + MWCNTs)

Khursheed Muhammad[1] · T. Hayat[1] · A. Alsaedi[2] · B. Ahmed[2]

Received: 27 July 2019 / Accepted: 16 September 2020 / Published online: 6 October 2020

Abstract

In this communication, we have investigated flow of hybrid nanomaterial (SWCNTs + MWCNTs) by a curved stretched surface. Relative analysis of nanomaterial (SWCNTs) and hybrid nanomaterial (SWCNTs + MWCNTs) is performed. Gasoline oil is treated as basefluid. Heat transfer features are elaborated via thermal radiation and convection. Equations relevant to flow field (PDEs) are transmitted into ODEs through adequate transformations. Solutions are developed via the shooting method. Furthermore, relative analysis of basefluid (gasoline oil), nanomaterial (SWCNTs) and hybrid nanomaterial (SWCNTs + MWCNTs) is presented through higher estimations of influential flow parameters during observation of flow, skin friction coefficient, temperature and Nusselt number.

Keywords Curved sheet · Convective boundary condition · Hybrid nanofluid (SWCNTs + MWCNTs) · Thermal radiation · Gasoline oil (basefluid) · Numerical solution

Abbreviations

u, v	Components of velocity
s, r	Curvilinear coordinates system
μ_f	Fluid dynamic viscosity
ν_f	Kinematic fluid viscosity
ρ_f	Density of basefluid
k_f	Fluid thermal conductivity
α_f	Thermal diffusivity of basefluid
f'	Non-dimensional velocity
θ	Non-dimensional temperature
CNTs	Carbon nanotubes
γ_0	Heat transfer coefficient
β	Thermal Biot number
γ	Curvature parameter
Rd	Radiation parameter
σ^*	Mean absorption coefficient

For hybrid nanofluid

μ_{hnf}	Dynamic viscosity
ν_{hnf}	Kinematic viscosity
ρ_{hnf}	Density
k_{hnf}	Thermal conductivity
α_{hnf}	Thermal diffusivity
$(c_p)_{hnf}$	Specific heat
$(c_p)_f$	Specific heat of basefluid
Pr	Prandtl number
τ_w	Wall shear stress
U_0	Arbitrary constants
p	Pressure
$U_w(s)$	Stretching surface velocity
P	Non-dimensional pressure
T_∞	Fluid ambient temperature
k_{S_1}	Thermal conductivity of SWCNTs
k_{S_2}	Thermal conductivity of MWCNTs
MWCNTs	Multiple-walled CNTs
SWCNTs	Single-walled CNTs
ϕ_2	MWCNTs volume fraction
ϕ_1	SWCNTs volume fraction
Q^*	Heat source/sink coefficient

For nanofluid

k_{nf}	Thermal conductivity
α_{nf}	Thermal diffusivity
$(c_p)_{nf}$	Specific heat
μ_{nf}	Dynamic viscosity
ν_{nf}	Kinematic viscosity
ρ_{nf}	Density

✉ Khursheed Muhammad
kmuhammad@math.qau.edu.pk; khursheedfaiq@gmail.com

[1] Department of Mathematics, Quaid-I-Azam University, Islamabad 44000, Pakistan

[2] Nonlinear Analysis and Applied Mathematics (NAAM) Research Group, Department of Mathematics, Faculty of Science, King Abdulaziz University, Jeddah, Saudi Arabia

Introduction

Recent developments in industrial and thermal processes directly depend upon the requirement of processing more compact and efficient heat transfer equipments. To fulfill such requirements the scientists and engineers have made many attempts to design various equipment and fluids for the advance of heat transfer rate. The consequence of such attempts is that solid materials are better thermal conductors when compared with liquids. Presently various liquids are used for cooling purposes as cooling agents. To improve thermal conductance of such liquids, the scientists and engineers added some small (nano) sized particles into it. Such nano-sized particles are referred as nanoparticles. Nanoparticles are made of metal (copper, gold etc.), carbides, oxides (alumina, titania) and copper oxides etc. Kerosine oil, ethylene glycol, bioliquids, water and some lubricants are utilized as traditional liquids. The suspension of such nano-sized particles in basematerial is known as nanofluid. There are various shapes of nanoparticles like cylindrical, spherical, blades, bricks etc. It has been observed that thermal conductance of base liquid highly depends upon nanoparticles shape. Better performance in terms of enhancing thermal conductance of the baseliquid is observed for cylindrical shape nanoparticles (nanotubes). Carbon nanotubes are cylindrical shape material with one (single-wall) or more (multi-wall) layers of graphene. There are extensive applications of CNTs in energy storages, microelectronics, coating and films, purification of drinking water, defense and sports materials etc. Initial analysis on nanofluid was performed by Choi and Eastman (1995). Applications of nanofluid comprises systems of drug delivery, refrigerant, solar collectors, solar cells and many more. Chemical reactions and melting phenomenon in flow of CNTs is presented by Hayat et al. (2018a). Khan et al. (2019) examined entropy production minimization in flow of Carreau nanomaterial. Chemical reactions, radiation and melting effect in flow of CNTs are studied by Hayat et al. (2018b). Heat generation and entropy production in MHD flow of nanomaterial is analyzed by Hosseini et al. (2019). Convection in flow of copper/water nanomaterial due to rotatory cone is examined by Dinarvand and Pop (2017). Melting heat, chemical reactions and radiation in flow of CNTs by a curved sheet in presented by Hayat et al. (2019a). Mahian et al. (2018) performed modern analysis in modeling and simulation of nanomaterial flow. Comparative analysis amongst nanomaterial, basefluid and hybrid nanomaterial is performed by Muhammad et al. (2020). Nowadays various experimental works has been performed by the researchers on dispersion of more than one nanoparticle in the same basefluid. This mixture of two or more nanoparticles and basefluid is referred as hybrid nanofluid. Hybrid nanofluid possesses better thermal features when compared with nanofluid. A review works on the development and applications of hybrid nanomaterial is performed by Sarkar et al. (2015). Some recent work on nanomaterial and hybrid nanomaterial can be seen in Hayat and Nadeem (2017), Huminic and Huminic (2019), Meribout (2019), Meribout et al. (2018, 2019), Xu et al. (2019a, b), Sajid and Ali (2018), Sun et al. (2019).

Flow due to the stretchable sheet is discussed extensively due to its wide range of technological as well as industrial applications. The quality of final produced material can be effected deeply by the heat transfer rate at the stretchable surface. In this domain, the initial study was performed by Crane (1970). Heat transport via melting phenomenon in flow Oldroyd-B material over a stretched sheet is studied by Hayat et al. (2018c). MHD and joule heating effect in Fe_3O_4-flow of nanomaterial is elaborate by Sajid et al. (2016). Hayat et al. (2019b) studied entropy production and activation energy in flow of Ree-Eyring nanomaterial over a stretching sheet. Blasious flow of nanomaterial using Buongiorno's model is investigated by Naveed et al. (2016). Some recent analyses on flow over stretched surface can be seen in Singeetham and Puttanna (2019), Ali et al. (2017), Muhammad et al. (2019).

Literature survey indicates that in previously published works the researchers have investigated the flow of nanomaterial over a flat stretchable surface. Very little work is addressed yet regarding hybrid nanomaterial. Motivation behind the presented investigation is to study the flow of hybrid nanofluid by a curved stretched surface. CNTs (SWCNTs, MWCNTs) are dispersed in basefluid of gasoline oil. Characteristics of heat transportation are elaborated via thermal radiation and convection. Solutions are developed by the shooting method. Relative analysis for basefluid (gasoline oil), nanomaterial (SWCNTs) and hybrid nanomaterial (SWCNTs + MWCNTs) is emphasized.

Formulations

We have assumed flow of hybrid nanomaterial (SWCNTs + MWCNTs) by a curved stretching surface. Heat transport features are analyzed in presence of thermal radiation and convection. Nanofluid is prepared by adding SWCNTs (single-walled CNTs) in basefluid of gasoline oil while hybrid nanofluid is constructed by adding CNTs (single-walled and multiple-walled) in basefluid of gasoline oil. In Curvilinear coordinates system, $s -$ axis is taken along thecurved sheet while $r -$ axis normal to it. Single-wall CNTs are treated as first while multiple-wall CNTs are treated as second nanoparticles. We have assumed velocity $\mathbf{V} = [v(r, s),$

$u(r, s)$, 0]. General forms of involved equations (continuity, momentum and energy) are (Muhammad et al. 2020):

$$\frac{\partial \rho}{\partial t} + \nabla \cdot (\rho \mathbf{V}) = 0, \tag{1}$$

$$\rho_{hnf}\left(\frac{\partial \mathbf{V}}{\partial t} + (\mathbf{V}\cdot\nabla)\mathbf{V}\right) = \nabla\cdot\boldsymbol{\tau} + \rho b, \tag{2}$$

$$(\rho c_p)_{hnf}\left(\frac{\partial T}{\partial t} + (\mathbf{V}\cdot\nabla)T\right) = \mathrm{Tr}(\boldsymbol{\tau}\cdot\mathbf{L}) - \nabla\cdot\mathbf{q} + \mathbf{q}_r. \tag{3}$$

In aforementioned expressions, Eq. (1) is referred as continuity equation. The derivation of this equation is based on conservations law of mass. Equation (2) is called the momentum equation. Derivation of this equation is based on Newton's second law. In this equation, left-hand side represents inertial forces while the first term on right-hand side is surface force and second term the body forces. Equation (3) is called the energy equation and its derivation is on the basis of the first law of thermodynamics. Here L.H.S represents total internal energy of the system while the first term on R.H.S is due to viscous dissipation, second for Fourier's law of heat conduction and a third term for radiated heat flux. Here $\mathbf{q} = -k_{hnf}\nabla T$ represents heat flux. We are interested in studying the two-dimensional flow of an incompressible hybrid nanofluid in absence of thermal radiation and viscous dissipation. Thus after implementing aforementioned assumptions, the expressions are:

$$(r+R)\frac{\partial v}{\partial r} + v + R\frac{\partial u}{\partial s} = 0, \tag{4}$$

$$\frac{u^2}{r+R} = \frac{1}{\rho_{hnf}}\frac{\partial p}{\partial r}, \tag{5}$$

$$v\frac{\partial u}{\partial r} + \frac{R}{r+R}u\frac{\partial u}{\partial s} + \frac{uv}{r+R} = -\frac{1}{\rho_{hnf}}\frac{R}{r+R}\frac{\partial p}{\partial s} + \upsilon_{hnf}\left(\frac{\partial^2 u}{\partial r^2} + \frac{1}{r+R}\frac{\partial u}{\partial r} - \frac{u}{(r+R)^2}\right), \tag{6}$$

$$\left(v\frac{\partial T}{\partial r} + \frac{R}{r+R}u\frac{\partial T}{\partial s}\right) = \frac{k_{hnf}}{(\rho c_p)_{hnf}}\left(\frac{1}{r+R}\frac{\partial T}{\partial r} + \frac{\partial^2 T}{\partial r^2}\right)\left(1 + \frac{16\sigma^* T_\infty}{3k^*}\right) + \frac{Q^*}{(\rho c_p)_{hnf}}(T - T_\infty), \tag{7}$$

with boundary conditions

$$u = U_w(s) = U_0 s, \quad v = 0, \quad -k_{hnf}\frac{\partial T}{\partial r} = \gamma_0(T_f - T) \text{ at } r = 0,$$
$$u \to 0, \quad T \to T_\infty \text{ as } r \to \infty. \tag{8}$$

We choose the transformations:

$$u = U_0 s f'(\eta), \quad v = -\frac{R}{r+R}\sqrt{\frac{U_0 \upsilon_f}{2l}}f(\eta), \quad \eta = \sqrt{\frac{U_0}{\upsilon_f}}r,$$
$$\theta(\eta) = \frac{T - T_\infty}{T_w - T_\infty}, \quad p = \rho_f U_0^2 s^2 P(\eta). \tag{9}$$

Implementing these transformations on the above flow expressions, continuity equation is verified identically while other equations with boundary conditions become:

$$P'(\eta) = A_{11}\frac{f'^2}{\eta+\gamma}, \tag{10}$$

$$\frac{2\gamma}{\eta+\gamma}P(\eta) = \frac{(1-\phi_1)^{2.5}(1-\phi_2)^{2.5}\frac{\gamma}{\eta+\gamma}}{A_{11}} \times \left(ff'' - f'^2 - \frac{\gamma}{\eta+\gamma}f'^2 + \frac{1}{\eta+\gamma}ff'\right) - \frac{f'}{(\eta+\gamma)^2} + \frac{f''}{\eta+\gamma} + f''', \tag{11}$$

$$(1+Rd)\frac{k_{hnf}}{k_f}\left(\theta'' + \frac{\theta'}{\eta+\gamma}\right) + B_{11}\,\mathrm{Pr}\left(\frac{\gamma}{\eta+\gamma}f\theta' + \delta\theta\right) = 0. \tag{12}$$

Elimination of $P(\eta)$ from Eqs. (10) and (11) yields

$$\frac{A_{11}}{(1-\phi_1)^{2.5}(1-\phi_2)^{2.5}}\left(f'''' + \frac{2}{\eta+\gamma}f''' + \frac{f'}{(\eta+\gamma)^3} - \frac{1}{(\eta+\gamma)^2}f''\right) + \frac{\gamma}{\eta+\gamma}\left(ff''' - f'f'' + \frac{ff''}{\eta+\gamma} - \frac{f'^2}{\eta+\gamma} - \frac{ff'}{(\eta+\gamma)^2}\right) = 0, \tag{13}$$

with

$$f'(0) = 1, \quad \theta'(0) = \frac{k_f}{k_{hnf}}\beta(1-\theta(0)), \quad f(0) = 0,$$
$$f'(\eta) \to 0, \quad f''(\eta) \to 0, \quad \theta(\eta) \to 0 \text{ as } \eta \to \infty, \tag{14}$$

$$A_{11} = \frac{1}{(1-\phi_2)\left((1-\phi_1) + \phi_1\frac{\rho_{s_1}}{\rho_f}\right) + \phi_2\frac{\rho_{s_2}}{\rho_f}}, \tag{15}$$

$$B_{11} = (1-\phi_2)\left((1-\phi_1) + \phi_1\frac{(\rho c_p)_{s_1}}{(\rho c_p)_f}\right) + \phi_2\frac{(\rho c_p)_{s_2}}{(\rho c_p)_f}. \tag{16}$$

Physical parameters involved in flow field are defined by

$$\gamma = \sqrt{\frac{U_0}{\upsilon_f}}R, \quad \mathrm{Pr} = \frac{\upsilon_f}{\alpha_f}, \quad \delta = \frac{Q^*}{U_0(\rho c_p)_f},$$
$$\beta = \frac{\gamma_0}{k_f}\sqrt{\frac{\upsilon_f}{U_0}}, \quad Rd = \frac{16\sigma^* T_\infty^3}{3k_f}. \tag{17}$$

Expression for C_{fs} (skin friction coefficient) and Nu_s (Nusselt number)

Dimensionless expression of C_{fs} and Nu_s are

$$C_{fs}=\frac{(\tau_w)_{r=0}}{\rho U_w^2},\quad \mathrm{Nu}_s=\frac{s(q_w)_{r=0}}{k_f(T_w-T_\infty)},\tag{18}$$

$$\tau_w=\mu_{hnf}\left(\frac{\partial u}{\partial r}-\frac{u}{r+R}\right),\quad q_w=-k_{hnf}\frac{\partial T}{\partial r}.\tag{19}$$

Non-dimensional version is

$$\sqrt{\mathrm{Re}_s}C_{fs}=\frac{1}{(1-\phi_1)^{2.5}(1-\phi_2)^{2.5}}\left(f''(0)-\frac{1}{\gamma}f(0)\right),\tag{20}$$

$$\frac{\mathrm{Nu}_s}{\sqrt{\mathrm{Re}_s}}=-\frac{k_{hnf}}{k_f}\theta'(0).\tag{21}$$

Here $Re_s=\frac{U_w(s)s}{\upsilon_f}$ is the local Reynold number.

Himelton–Crosser model for hybrid nanofluid and nanofluid

Himelton–Crosser expressions for nanofluid and hybrid nanofluid are (Hayat and Nadeem 2017)

$$\begin{aligned}&\rho_{nf}=\left(1-\phi_1\right)\rho_f+\phi_1\rho_{s_1},\\&(\rho c_p)_{nf}=\left(1-\phi_1\right)(\rho c_p)_f+\phi_1(\rho c_p)_{s_1},\\&\frac{\kappa_{nf}}{\kappa_f}=\frac{\kappa_{s_1}+(n-1)\kappa_f-(n-1)\phi_1(\kappa_f-\kappa_{s_1})}{\kappa_{s_1}+(n-1)\kappa_f+\phi_1(\kappa_f-\kappa_{s_1})},\\&\mu_{nf}=\frac{\mu_f}{\left(1-\phi_1\right)^{2.5}},\ \upsilon_{nf}=\frac{\mu_{nf}}{\rho_{nf}},\end{aligned}\tag{22}$$

and

$$\begin{aligned}&\rho_{hnf}=\left(1-\phi_2\right)\left(\left(1-\phi_1\right)\rho_f+\phi_1\rho_{s_1}\right)+\phi_2\rho_{s_2},\\&(\rho c_p)_{hnf}=\left(1-\phi_2\right)\left(\left(1-\phi_1\right)(\rho c_p)_f+\phi_1(\rho c_p)_{s_1}\right)+\phi_{2(\rho c_p)_{s_2}},\\&\frac{\kappa_{hnf}}{\kappa_{nf}}=\frac{\kappa_{s_2}+(n-1)\kappa_{nf}-(n-1)\phi_2(\kappa_{nf}-\kappa_{s_2})}{\kappa_{s_2}+(n-1)\kappa_{nf}+\phi_2(\kappa_{nf}-\kappa_{s_2})},\\&\frac{\kappa_{nf}}{\kappa_f}=\frac{\kappa_{s_1}+(n-1)\kappa_f-(n-1)\phi_1(\kappa_f-\kappa_{s_1})}{\kappa_{s_1}+(n-1)\kappa_f+\phi_1(\kappa_f-\kappa_{s_1})},\\&\mu_{hnf}=\frac{\mu_f}{\left(1-\phi_1\right)^{2.5}\left(1-\phi_2\right)^{2.5}},\ \upsilon_{hnf}=\frac{\mu_{hnf}}{\rho_{hnf}}.\end{aligned}\tag{23}$$

In the above expressions, n is known by shape parameter such that $n=6$ represents cylindrical-shaped nanoparticles. Thus in our analysis, we have taken $n=6$.

Method for solutions

The coupled non-linear ODEs are solved by shooting technique using with Runge–Kutta 4th-order algorithm (bvp4c: A matlab tool). This technique is applicable for first order ODEs. Thus we have adopted this method as $y_0=f$,

$$y_1=f',\tag{24}$$

$$y_2=f'',\tag{25}$$

$$y_3=f''',\tag{26}$$

$$\begin{aligned}Y_0=y_3'=&-A_{11}(1-\phi_1)^{2.5}(1-\phi_2)^{2.5}\frac{\gamma}{\eta+\gamma}\\&\times\left(y_0y_3-y_1y_2+\frac{y_0y_2}{\eta+\gamma}-\frac{y_1^2}{\eta+\gamma}-\frac{y_0y_1}{(\eta+\gamma)^2}\right)\\&-\frac{2\gamma}{\eta+\gamma}y_3-\frac{y_1}{(\eta+\gamma)^3}+\frac{y_2}{(\eta+\gamma)^2},\end{aligned}\tag{27}$$

$$y_4=\theta,\tag{28}$$

$$y_5=\theta',\tag{29}$$

$$Y_1=y_5'=-\frac{B_{11}}{1+Rd}\frac{k_f}{k_{hnf}}\Pr\left(\frac{\gamma}{\eta+\gamma}y_0y_5+\delta y_4\right)-\frac{y_5}{\eta+\gamma},\tag{30}$$

with

$$\begin{aligned}&y_1(0)=1,\quad y_5(0)=\frac{k_f}{k_{hnf}}\beta(1-y_4(0)),\quad y_0(0)=0,\\&y_1\to0,\quad y_2\to0,\ y_4\to0\text{ as }\eta\to\infty.\end{aligned}\tag{31}$$

Analysis

Aim behind this analysis section is to perform or to elaborate relative study among basefluid (gasoline oil), nanomaterial (SWCNTs) and hybrid nanomaterial (SWCNTs + MWCNTs). C_{fs} (Skin friction coefficient), $f'(\eta)$ (velocity of fluid), $\theta(\eta)$ and Nu_s (Nusselt number) are graphically visualized against higher estimations of $\beta,\ \phi_1,\ \gamma,\phi_2$ and Rd. Such graphical analysis is performed as below:

1. a-graphs are plotted for relative analysis between nanomaterial (SWCNTs) and hybrid nanomaterial (SWCNTs + MWCNTs) corresponding to each physical parameter.
2. b-graphs are plotted for relative analysis among base-fluid (gasoline oil), nanomaterial (SWCNTs) and hybrid nanomaterial (SWCNTs + MWCNTs).

Analysis of velocity ($f'(\eta)$)

Flow ($f'(\eta)$) against the larger estimation of ϕ_1 during relative analysis of nanomaterial (SWCNTs) and hybrid nanomaterial (SWCNTs + MWCNTs) is presented in Fig. 1. Velocity $f'(\eta)$ is maximized with increment in ϕ_1. Also prominent impact is shown by a hybrid nanofluid. Volocity $f'(\eta)$ due to larger values of γ is sketched in Fig. 2. Direct relation between $f'(\eta)$ and γ is observed. Physically an increment in a radius of curved surface occurs with higher γ. Thus more fluid particles attain stretched surface velocity and thus $f'(\eta)$ enhances. However, the prominent effect for hybrid nanofluid (SWCNTs + MWCNTs) is noticed. Figure 3 is plotted for relative analysis of nanomaterial (SWCNTs) and hybrid nanomaterial (SWCNTs + MWCNTs) during studying impact for higher ϕ_2 on $f'(\eta)$. Velocity $f'(\eta)$ increases with larger ϕ_2 and prominent impact is detected for hybrid nanofluid. Relative analysis for basefluid (gasoline oil), nanofluid (SWCNTs) and hybrid nanofluid (SWCNTs + MWCNTs) about $f'(\eta)$ when $\phi_1 = \phi_2 = 0.1$ is presented in Figs. 4, 5, 6, respectively. As expected the prominent behavior is noticed for hybrid nanofluid (SWCNTs + MWCNTs) followed by nanofluid (SWCNTs) and basefluid (gasoline oil), respectively.

Analysis for $\theta(\eta)$ (temperature)

Temperature of the fluid ($\theta(\eta)$) via higher estimation of ϕ_1 is labeled in Fig. 7. Direct behavior is noticed for $\theta(\eta)$ via higher ϕ_1. Physically an increment in ϕ_1 intensifies thermophysical characteristics of basefluid due to which

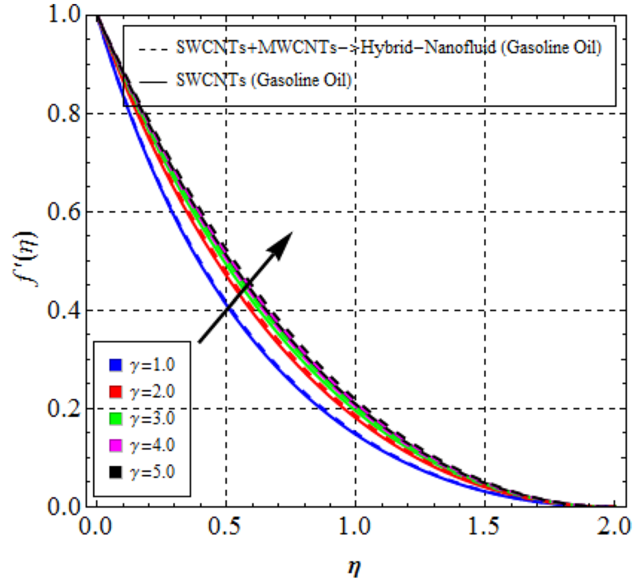

Fig. 2 $f'(\eta)$ vs γ

convective flow from heated surface towards cold fluid intensifies. Hence $\theta(\eta)$ increases. Furthermore, impact of hybrid nanofluid (SWCNTs + MWCNTs) is dominant. Figure 8 is plotted for variation in $\theta(\eta)$ against increment in γ. Temperature $\theta(\eta)$ enhances with enlargement in γ and dominant behavior is noticed for nanofluid (SWCNTs). Variations in $\theta(\eta)$ due to higher estimation of β is portrayed in Fig. 9.Temperature $\theta(\eta)$ directly varies with increasing values of β. Physically higher β correspond to an increase in rate of heat transfer and thus $\theta(\eta)$ increases. Moreover, the impact of nanofluid (SWCNTs) is prominent

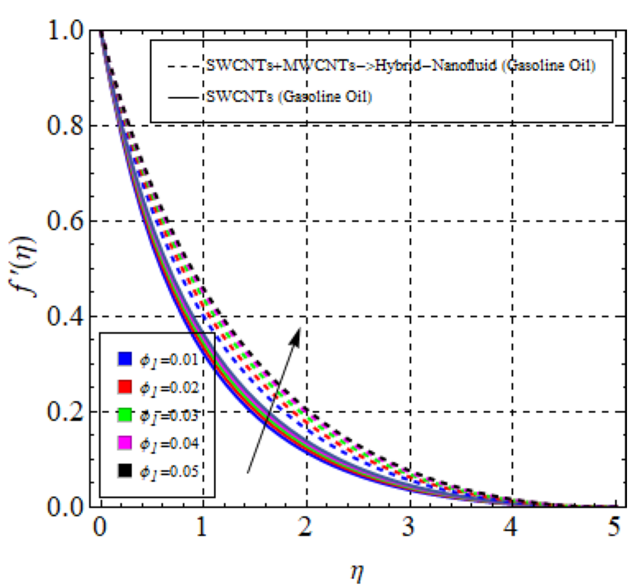

Fig. 1 $f'(\eta)$ vs ϕ_1

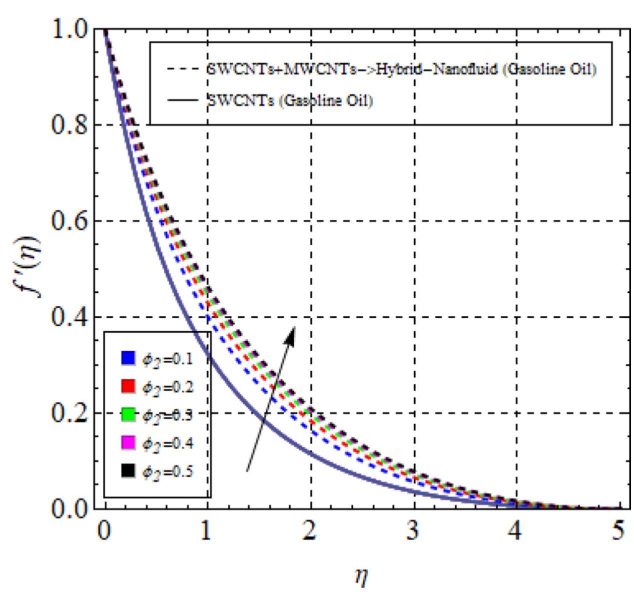

Fig. 3 $f'(\eta)$ vs ϕ_2

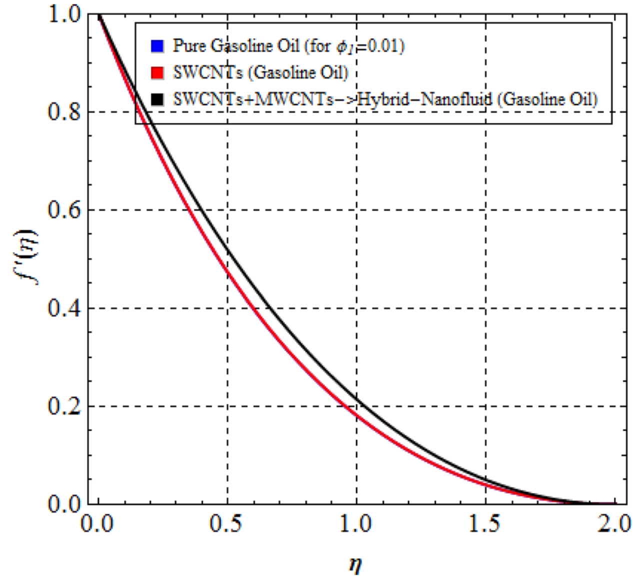

Fig. 4 $f'(\eta)$ vs ϕ_1 (compraison)

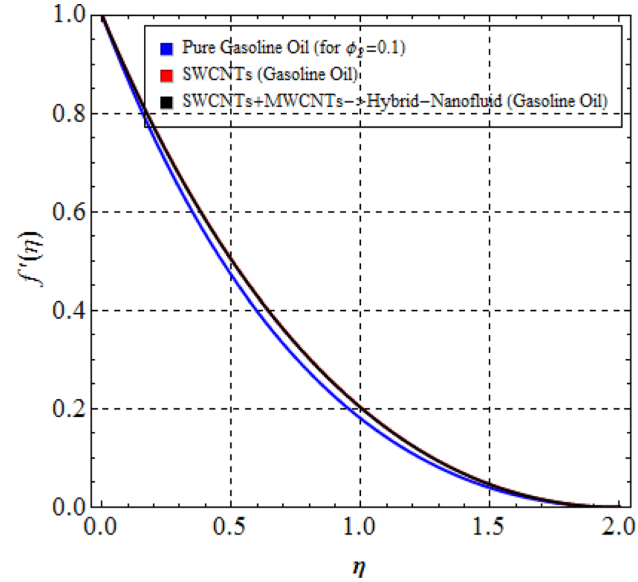

Fig. 6 $f'(\eta)$ vs γ (compraison)

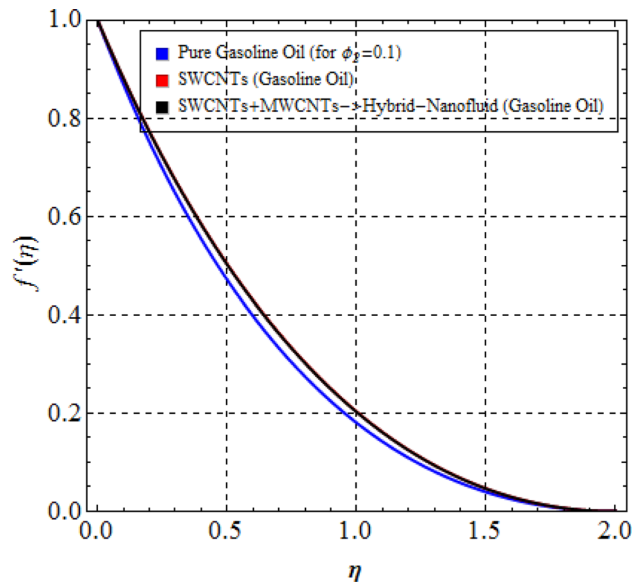

Fig. 5 $f'(\eta)$ vs ϕ_2 (compraison)

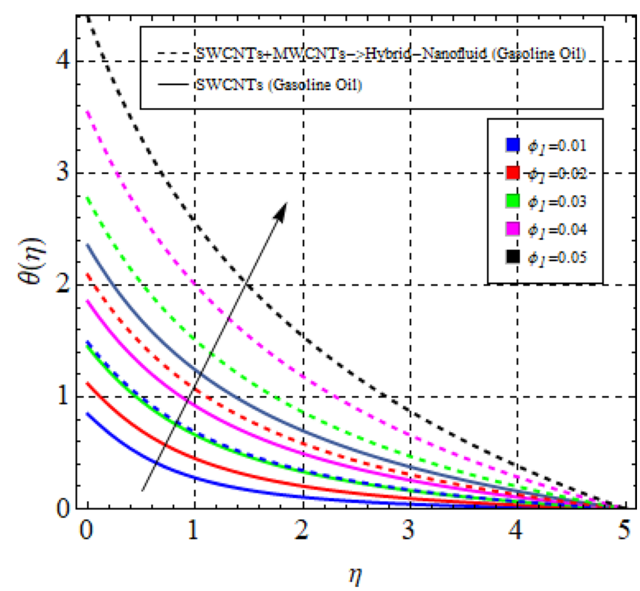

Fig. 7 $\theta(\eta)$ vs ϕ_1

when compared with hybrid nanofluid (SWCNTs + MWCNTs). Figure 10 is sketched for variations in $\theta(\eta)$ against higher Rd. Enlargement in $\theta(\eta)$ is observed for higher Rd. Physically higher Rd leads to the production of more heat via radiation process and so $\theta(\eta)$ intensifies. Nanofluid (SWCNTs) shows prominent impacts as compared to hybrid nanofluid (SWCNTs + MWCNTs). Figure 11 is labeled for variations in $\theta(\eta)$ due to higher estimation of ϕ_2. It is noticed that $\theta(\eta)$ intensifies with enlargement in ϕ_2. Higher ϕ_2 is associated with a more convective flow from the heated surface towards cold fluid above the surface. Thus $\theta(\eta)$ intensifies. Furthermore, the impact of hybrid nanomaterial (SWCNTs + MWCNTs) is dominant over nanofluid (SWCNTs). Temperature $\theta(\eta)$ against $\delta > 0$ (heat source parameter) and $\delta < 0$ (heat sink parameter) is plotted in Fig. 12. It is revealed that $\theta(\eta)$ intensifies for $\delta > 0$ while it reduces for $\delta < 0$. Further influence of nanofluid (SWCNTs) is more when compared with hybrid nanofluid (SWCNTs + MWCNTs). Figures 13, 14, 15, 16, 17, 18 presents relative study among basefluid (gasoline

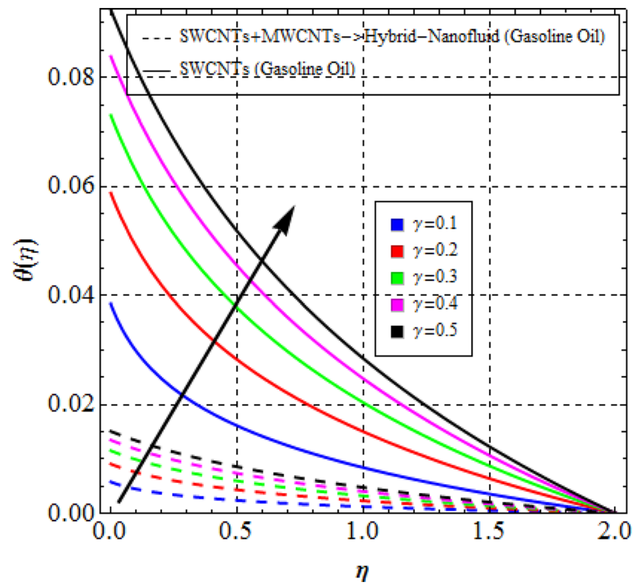

Fig. 8 $\theta(\eta)$ vs γ

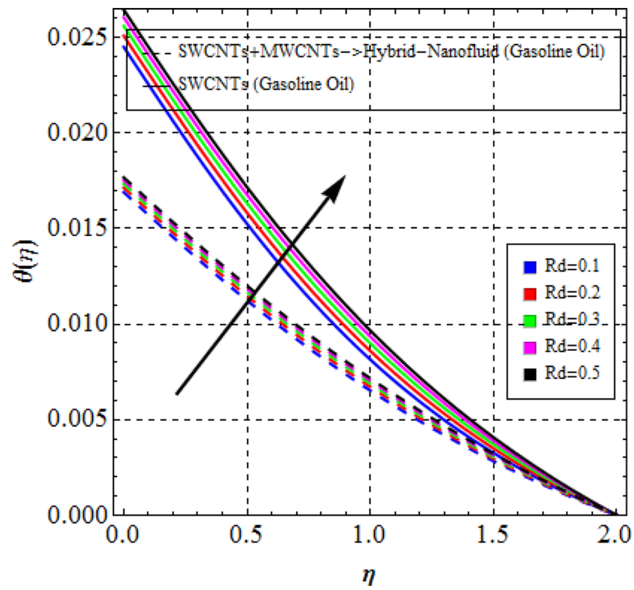

Fig. 10 $\theta(\eta)$ vs Rd

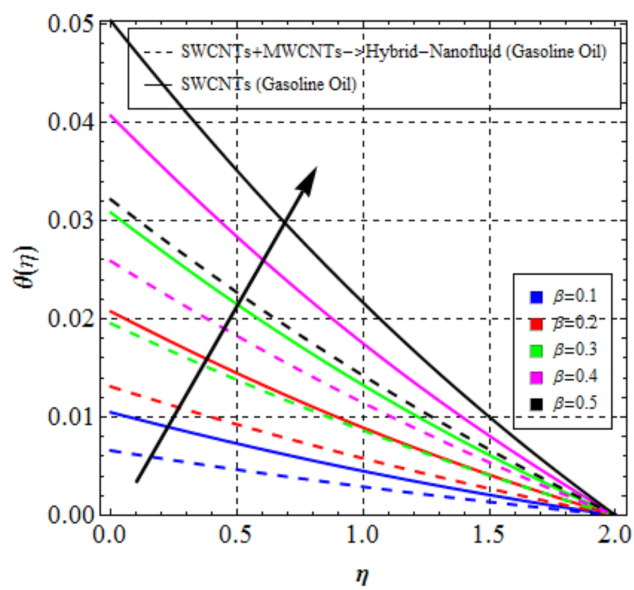

Fig. 9 $\theta(\eta)$ vs β

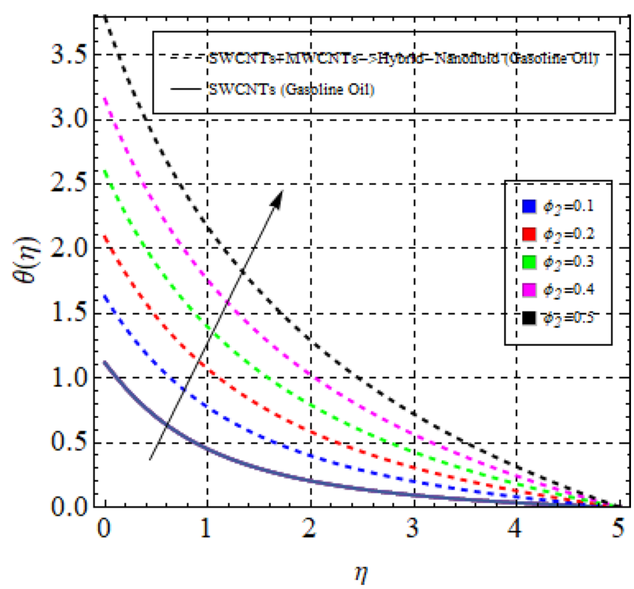

Fig. 11 $\theta(\eta)$ vs ϕ_2

oil), nanomaterial (SWCNTs) and hybrid nanomaterial (SWCNTs + MWCNTs) during the analysis of $\theta(\eta)$ when $\phi_1 = 0.01$ and $\gamma = \beta = \phi_2 = Rd = \delta = 0.1$, respectively. It is dugout that performance of hybrid nanomaterial (SWCNTs + MWCNTs) is better which is followed by nanofluid (SWCNTs) and basefluid (gasoline oil) when $\phi_1 = 0.01$ and $\phi_2 = 0.1$ while the impact of basefluid (gasoline oil) is massive which is followed by nanofluid (SWCNTs) and hybrid nanofluid (SWCNTs + MWCNTs) when $\gamma = \beta = Rd = \delta = 0.1$.

Analysis of C_{fs} (skin friction coefficient) and Nu_s (Nusselt number)

C_{fs} against higher estimations of ϕ_1, ϕ_2 and γ is portrayed in Figs. 19, 20. It is founded that C_{fs} enhances both ϕ_1 and ϕ_2 while it decays with higher γ. Further impact of

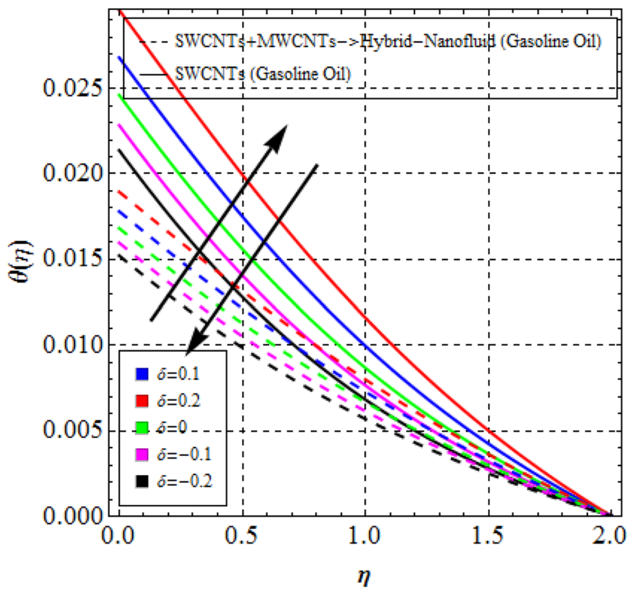

Fig. 12 $\theta(\eta)$ vs δ

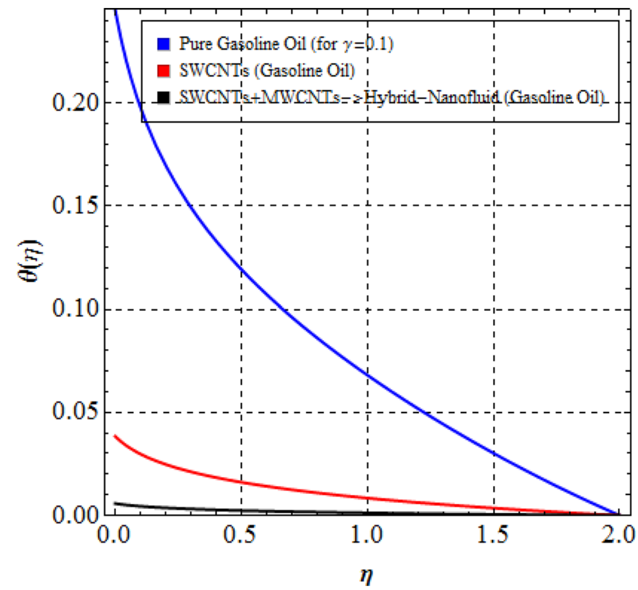

Fig. 14 $\theta(\eta)$ vs γ (comparison)

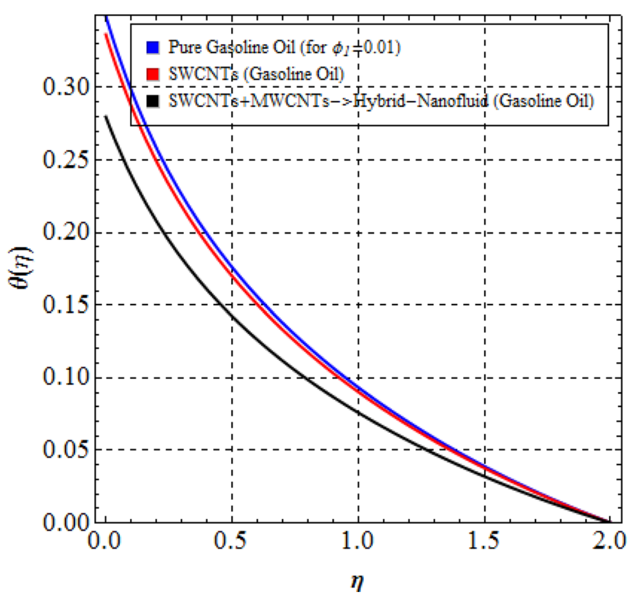

Fig. 13 $\theta(\eta)$ vs ϕ_1 (comparison)

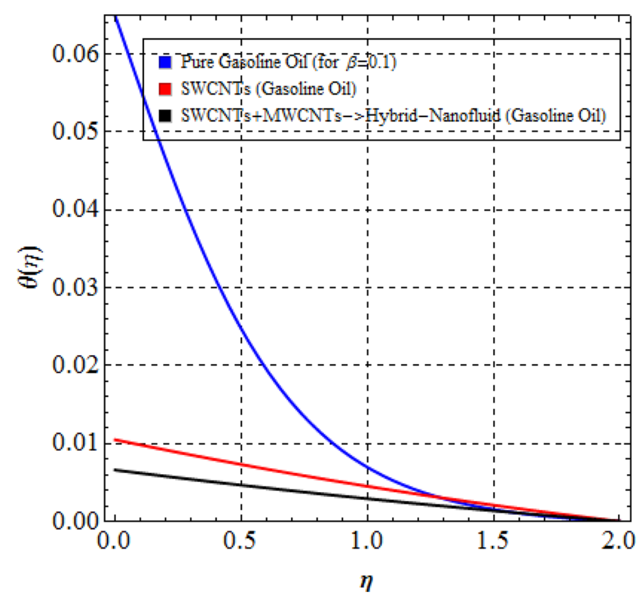

Fig. 15 $\theta(\eta)$ vs β (comparison)

hybrid nanomaterial (SWCNTs + MWCNTs) is more than nanomaterial (SWCNTs). Relative analysis of basefluid (gasoline oil), nanomaterial (SWCNTs) and hybrid nanomaterial (SWCNTs + MWCNTs) during computation of C_{fs} when $\gamma = \phi_1 = 0.1$ is performed in Figs. 21, 22. Better performance is seen for hybrid nanomaterial (SWCNTs + MWCNTs) followed by nanomaterial (SWCNTs) and basefluid (gasoline oil), respectively. However, for $\phi_2 = 0.1$ the basefluid (gasoline oil) result is followed by nanofluid (SWCNTs) and hybrid nanofluid (SWCNTs). Nu_s against higher γ, β, ϕ_1 and ϕ_2 is labeled in Figs. 23 and 24. It is found that Nu_s intensifies with higher γ, β, ϕ_1 and ϕ_2. Moreover, the impact of hybrid nanomaterial (SWCNTs + MWCNTs) is more than nanomaterial (SWCNTs).

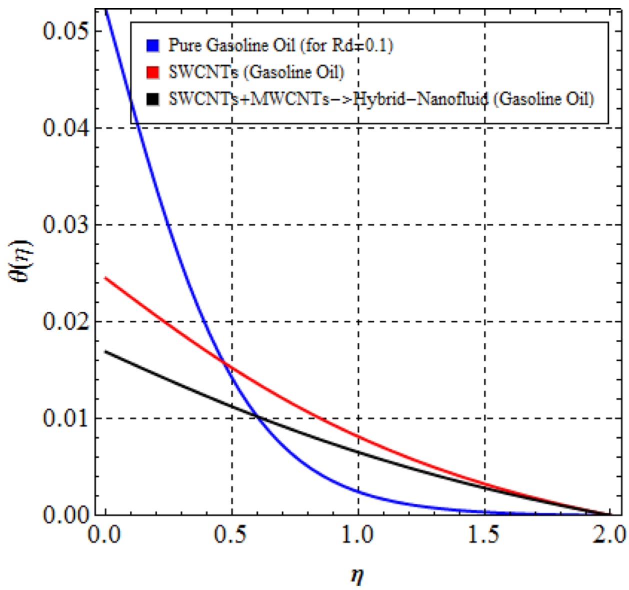

Fig. 16 $\theta(\eta)$ vs Rd (comparison)

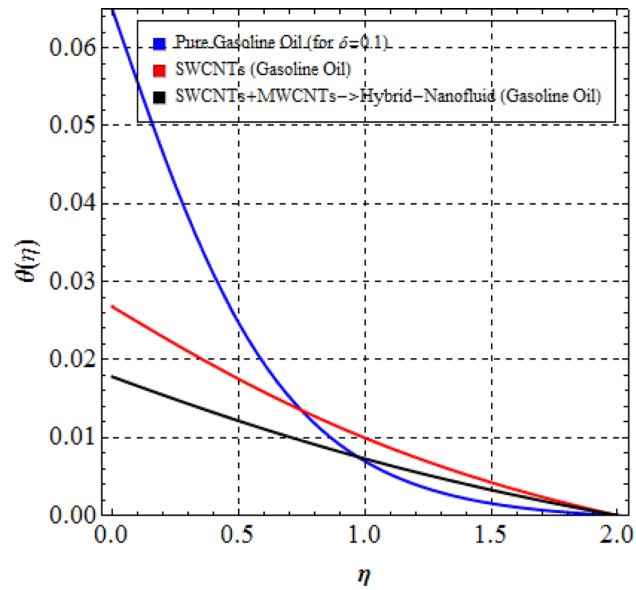

Fig. 18 $\theta(\eta)$ vs δ (comparison)

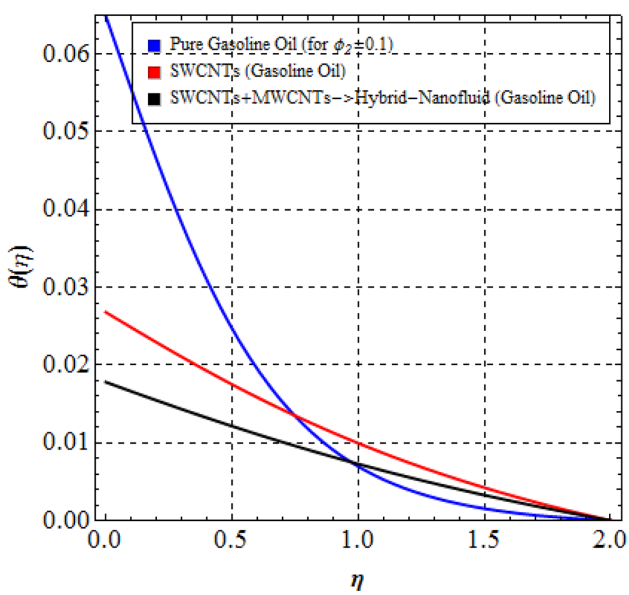

Fig. 17 $\theta(\eta)$ vs ϕ_2 (comparison)

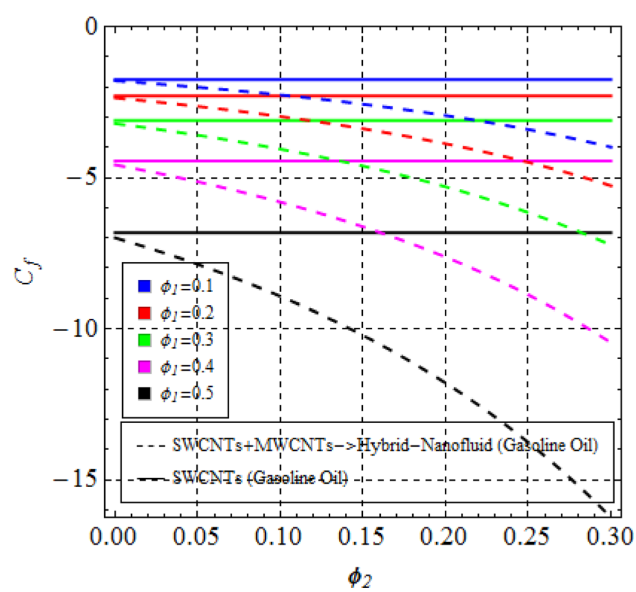

Fig. 19 C_f vs ϕ_1 and ϕ_2

Figures 25, 26 are sketched for the relative study of basefluid (gasoline oil), nanomaterial (SWCNTs) and hybrid nanofluid (SWCNTs + MWCNTs) during computation of Nu_s when $\gamma = \phi_1 = 0.1$. Efficient behavior is observed for hybrid nanomaterial (SWCNTs + MWCNTs) followed by nanomaterial (SWCNTs) and basefluid (gasoline oil).

Nomenclature of involved physical parameters and expressions is presented in Abbreviations. Table 1 is constructed for thermal features of CNTs (SWCNTs + MWCNTs) and basefluid (gasoline oil).

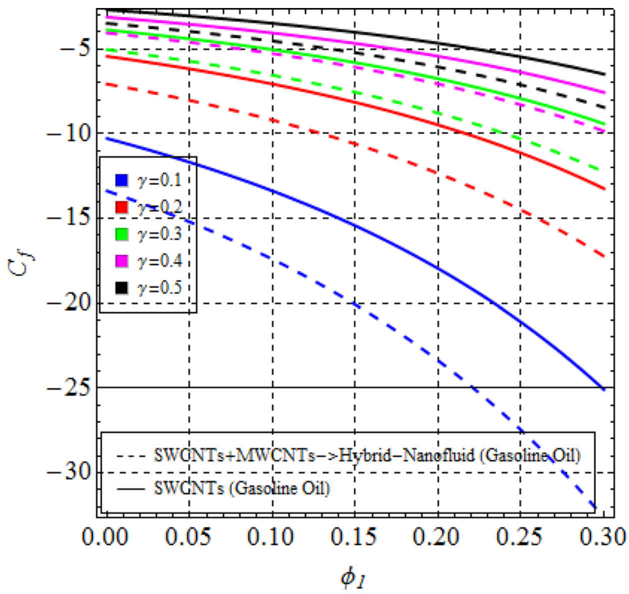

Fig. 20 C_f vs γ and ϕ_2

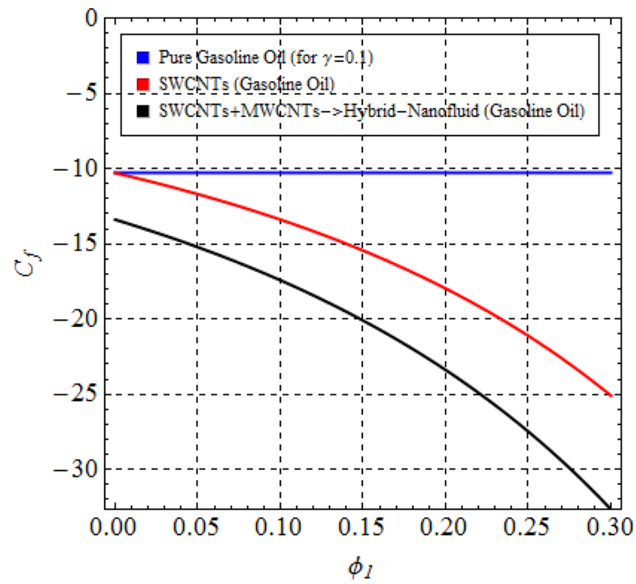

Fig. 22 C_f vs γ and ϕ_2 (comparison)

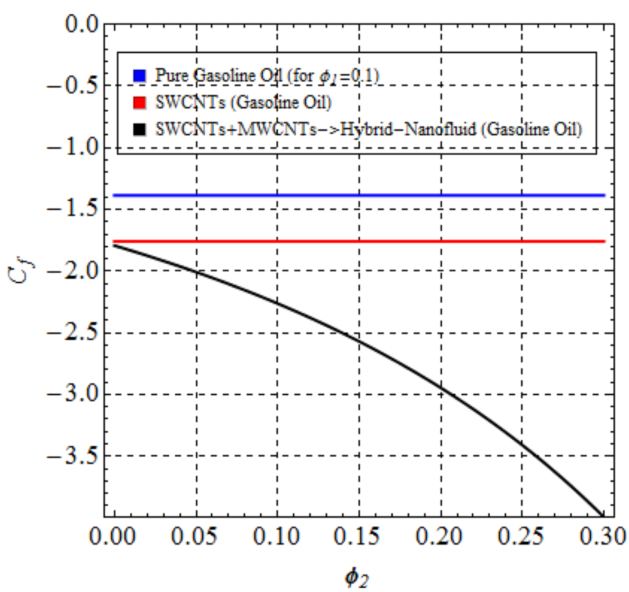

Fig. 21 C_f vs γ and ϕ_2 (comparison)

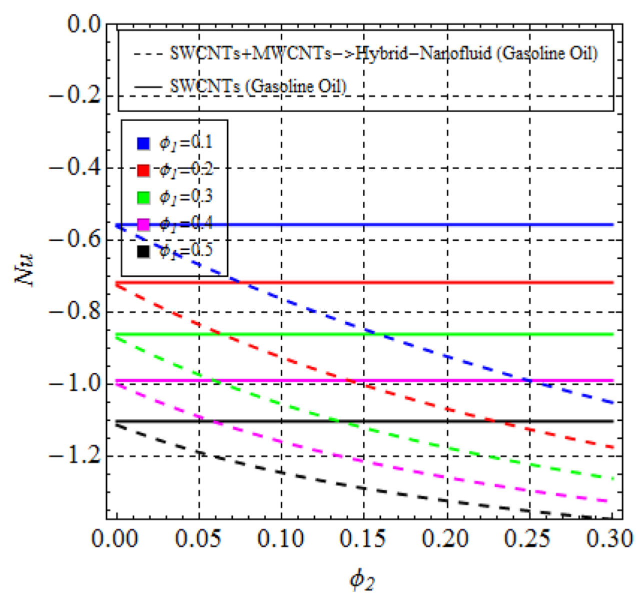

Fig. 23 Nu vs ϕ_1 and ϕ_2

Final findings

In presented work, we have examined flow of hybrid nanofluid (SWCNTs, MWCNTs) by a curved stretching sheet. The vital findings are.

Higher $f'(\eta)$ (velocity of fluid) is noticed with increment in ϕ_1, γ and ϕ_2.

$\theta(\eta)$ (temperature of fluid) rises with increment in values of γ, β and Rd while opposite behavior of $\theta(\eta)$ is seen with increment in ϕ_1 and ϕ_2.

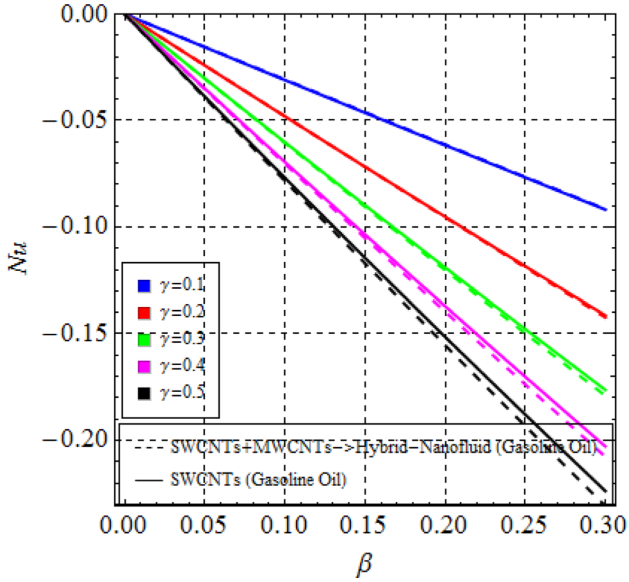

Fig. 24 Nu vs γ and β

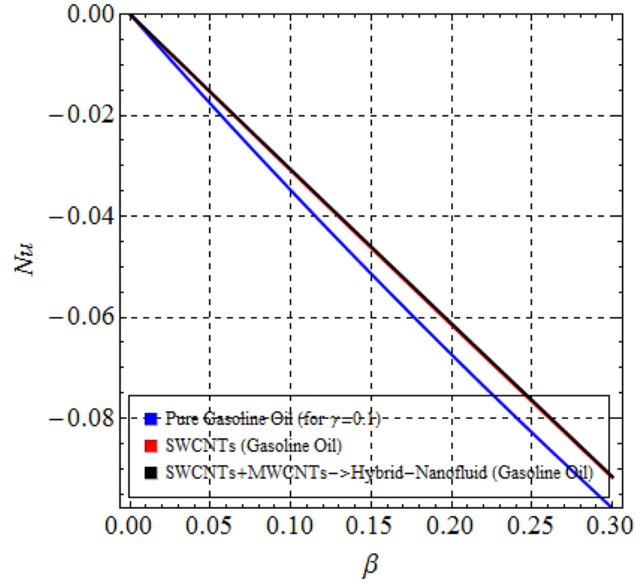

Fig. 26 Nu vs γ and β (comparison)

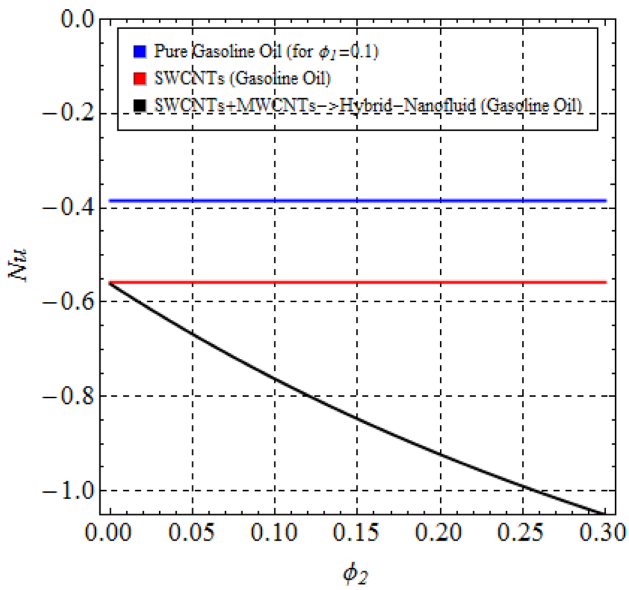

Fig. 25 Nu vs ϕ_1 and ϕ_2 (comparison)

Accurately $\theta(\eta)$ rises with heat source parameter ($\delta > 0$) while it decays with heat sink parameter ($\delta < 0$).

C_f (Skin friction coefficient) enlarges with increment in values of ϕ_1 and ϕ_2 while it reduces with γ.

Nu_s (Nusselt number) intensifies with increment in values of γ, β, ϕ_1 and ϕ_2.

Impacts of hybrid nanomaterial (SWCNTs + MWCNTs) are more than nanomaterial (SWCNTs) and basefluid (gasoline oil).

Table 1 Thermal features of CNTs (single-walled, multiple-walled) and basefluid (gasoline oil) (Crane 1970)

Nanoparticles\ thermophysical properties	$\rho\left(\frac{\mathrm{kg}}{\mathrm{m}^3}\right)$	$c_p\left(\frac{\mathrm{J}}{\mathrm{kgK}}\right)$	$\kappa\left(\frac{\mathrm{W}}{\mathrm{mK}}\right)$	Pr
SWCNTs	2600	425	6600	–
MWCNTs	1600	796	3000	–
Gasoline oil	884	1910	0.144	6450

Compliance with ethical standards

Conflict of interest The authors declare no conflict of competing interest.

References

Ali N, Khan SU, Sajid M, Abbas Z (2017) Slip effects in the hydromagnetic flow of a viscoelastic fluid through porous medium over a porous oscillatory stretching sheet. J Porous Media 20:249–262

Choi SUS, Eastman JA (1995) Enhancing thermal conductivity of fluids with nanoparticles. In: The proceedings of the 1995 ASME International Mechanical Engineering Congress and Exposition, vol 66, San Francisco ASME, FED 231/MD, pp 99–105

Crane LJ (1970) Flow past a stretching plate. J Appl Math Phys (ZAMP) 21:645–647

Dinarvand S, Pop I (2017) Free-convective flow of copper/water nanofluid about a rotating down-pointing cone using Tiwari-Das nanofluid scheme. Adv Powder Technol 28:900–909

Hayat T, Nadeem S (2017) Heat transfer enhancement with Ag-CuO/water hybrid nanofluid. Results Phys 7:2317–2324

Hayat T, Muhammad K, Alsaedi A, Asghar S (2018a) Numerical study for melting heat transfer and homogeneous-heterogeneous reactions in flow involving carbon nanotubes. Results Phys 8:415–421

Hayat T, Muhammad K, Muhammad T, Alsaedi A (2018b) Melting heat in radiative flow of carbon nanotubes with homogeneous-heterogeneous reactions. Commun Ther Phys 69:441–448

Hayat T, Muhammad K, Alsaedi A, Asghar S (2018c) Thermodynamics by melting in flow of an Oldroyd-B material. J Braz Soc Mech Sci Eng 40:530. https://doi.org/10.1007/s40430-018-1447-3

Hayat T, Muhammad K, Khan MI, Alsaedi A (2019a) Theoretical investigation of chemically reactive flow of water-based carbon nanotubes (single-walled and multiple walled) with melting heat transfer Pramana. J Phys. https://doi.org/10.1007/s12043-019-1722-6

Hayat T, Khan SA, Khan MI, Alsaedi A (2019b) Theoretical investigation of Ree-Eyring nanofluid flow with entropy optimization and Arrhenius activation energy between two rotating disks. Comput Methods Programs Biomed 177:57–68

Hosseini SR, Ghasemian M, Sheikholeslami M, Shafee A, Li Z (2019) Entropy analysis of nanofluid convection in a heated porous microchannel under MHD field considering solid heat generation. Powder Technol 344:914–925

Huminic G, Huminic A (2019) The influence of hybrid nanofluids on the performances of elliptical tube: recent research and numerical study. Int J Heat Mass Transf 129:132–143

Khan MI, Kumar A, Hayat T, Waqas M, Singh R (2019) Entropy generation in flow of Carreau nanofluid. J Mol Liq 278:677–687

Mahian O, Kolsi L, Amani M, Estellé P, Ahmadi G, Kleinstreuer C, Marshall JS, Siavashi M, Taylor RA, Niazmand H, Wongwises S, Hayat T, Kolanjiyil A, Kasaeian A, Pop I (2018) Recent advances in modeling and simulation of nanofluid flows-part I: fundamentals and theory. Phys Rep. https://doi.org/10.1016/j.physrep.2018.11.004

Meribout M (2019) Optimal design for a portable NMR and MRI-based multiphase flow meter. IEEE Trans Industr Electron 66:6354–6361

Meribout M, Saied IM, Hosani EA (2018) A new FPGA-based terahertz imaging device for multiphase flow metering. IEEE Transact Terahertz Sci Technol 8:418–426

Meribout M, Shehaz F, Saied IM, Bloohsi QA, AlAmri A (2019) High gas void fraction flow measurement and imaging using a THz-based device. IEEE Transact Terahertz Sci Technol 9:659–668

Muhammad K, Hayat T, Alsaedi A, Asghar S (2019) Stagnation point flow of basefluid (gasoline oil), nanomaterial (CNTs) and hybrid nanomaterial (CNTs+CuO): a comparative study. Mater Res Express. https://doi.org/10.1088/2053-1591/ab356e

Muhammad K, Hayat T, Alsaedi A, Ahmad B, Momani S (2020) Mixed convective slip flow of hybrid nanofluid (MWCNTs + Cu + Water), nanofluid (MWCNTs + Water) and base fluid (Water): a comparative investigation. J Ther Anal Calorim. https://doi.org/10.1007/s10973-020-09577-z

Naveed M, Abbas Z, Sajid M (2016) Thermophoresis and Brownian effects on the Blasius flow of a nanofluid due to a curved surface with thermal radiation. Euro Phys J Plus 131:1–9

Sajid MU, Ali HM (2018) Thermal conductivity of hybrid nanofluids: a critical review. Int J Heat Mass Transf 126:211–234

Sajid M, Iqbal SA, Naveed M, Abbas Z (2016) Joule heating and magnetohydrodynamic effects on ferrofluid (Fe3O4) flow in a semi-porous curved channel. J Mol Liq 222:1115–1120

Sarkar J, Ghosh P, Adil A (2015) A review on hybrid nanofluids: recent research, development and applications. Renew Sustain Energy Rev 43:164–177

Singeetham PK, Puttanna VK (2019) Viscoplastic fluids in 2D plane squeeze flow: a matched asymptotics analysis. J Nonnewton Fluid Mech 263:154–175

Sun B, Zhang Y, Yang D, Li H (2019) Experimental study on heat transfer characteristics of hybrid nanofluid impinging jets. Appl Therm Eng 151:556–566

Xu Y, Hu X, Kundu S, Nag A, Afsarimanesh N, Sapra S, Mukhopadhyay SC, Han T (2019a) Silicon-based sensors for biomedical applications: a review. Sensors (Basel). https://doi.org/10.3390/s19132908

Xu K, Chen Y, Okhai TA, Snyman LW (2019b) Micro optical sensors based on avalanching silicon light-emitting devices monolithically integrated on chips. Opt Mater Express 9:3985–3997